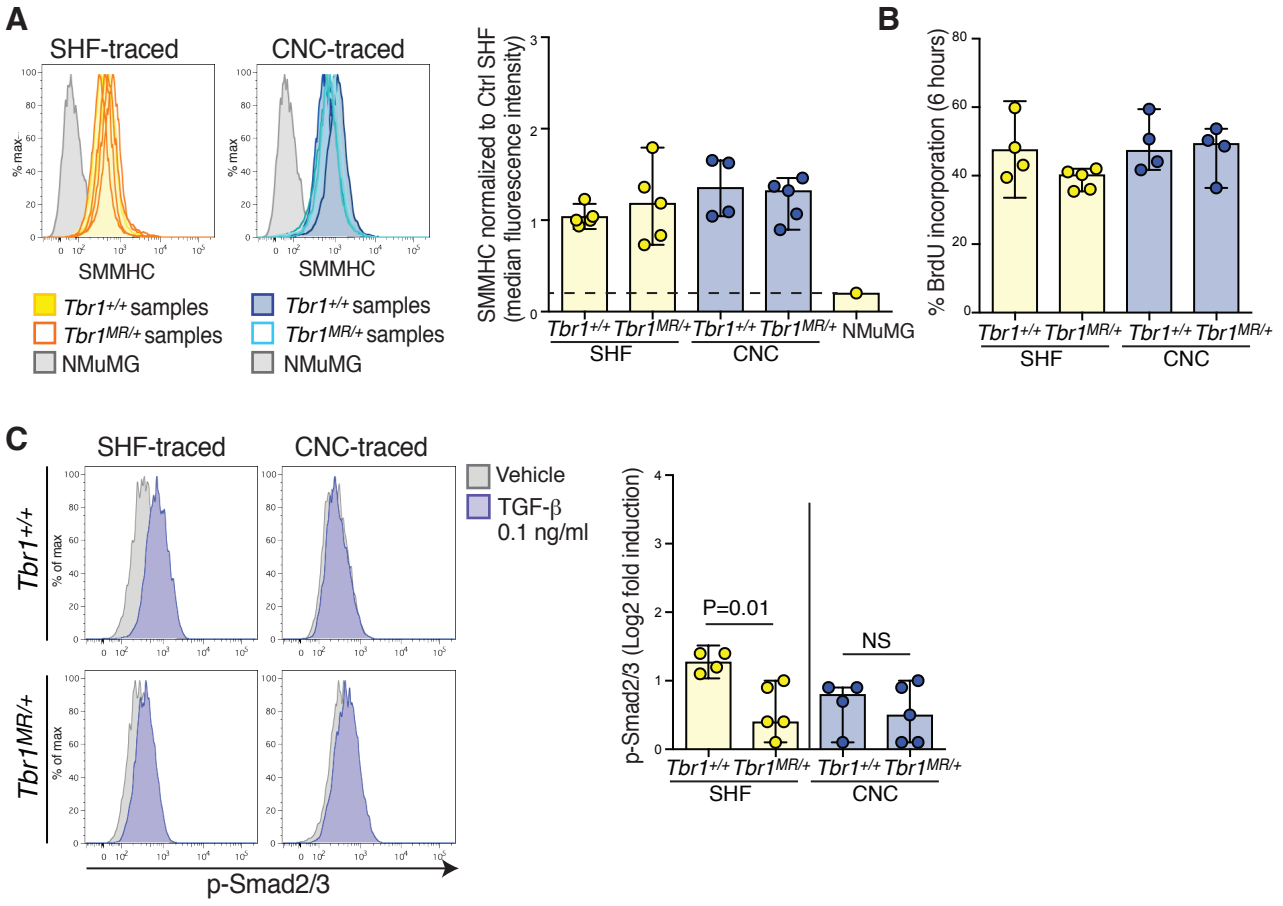

Supplementary Figure 1. Defective induction of p-Smad2/3 in response to 0.1 ng/ml TGF-β1 in SHF-, but not in CNC-derived VSMCs generated from *Tbr1*$^{MR/+}$ mice.

(**A**) Histogram plots and quantification of smooth muscle myosin heavy chain (SMMHC) expression as assessed by intracellular flow cytometry in control (*Tbr1*$^{+/+}$) and mutant (*Tbr1*$^{MR/+}$) SHF- and CNC-derived VSMCs, and in the NMuMG epithelial cell line (negative control) (SHF samples: control n=5, mutant n=5; CNC samples, control n=4, mutant n=5). No significant differences were found between lineage-traced VSMCs. (**B**) Quantification of bromodeoxyuridine (BrdU) incorporation as assessed by intracellular flow cytometry in SHF- and CNC-derived VSMCs of the indicated genotypes (SHF samples: control n=4, mutant n=5; CNC samples, control n=4, mutant n=4). No significant differences were found. (**C**) Flow cytometry histogram plot and quantification of p-Smad2/3 induction over baseline in serum-starved SHF- and CNC-derived VSMCs from mice of the indicated genotypes after exposure to 0.1 ng/ml of TGF-β1 for 1 hour. Levels of p-Smad2/3 were assessed by phospho-flow cytometry using an antibody specific for p-Smad2/3 (SHF samples: control n=4, mutant n=5; CNC samples, control n=4, mutant n=4). *P* values shown refer to Kruskal-Wallis test with FDR-based multiple comparison correction. Numerical data are presented as scatter dot-plots with boxes, with the box denoting the mean; error bars identify the 95% confidence interval. NS, not significant.

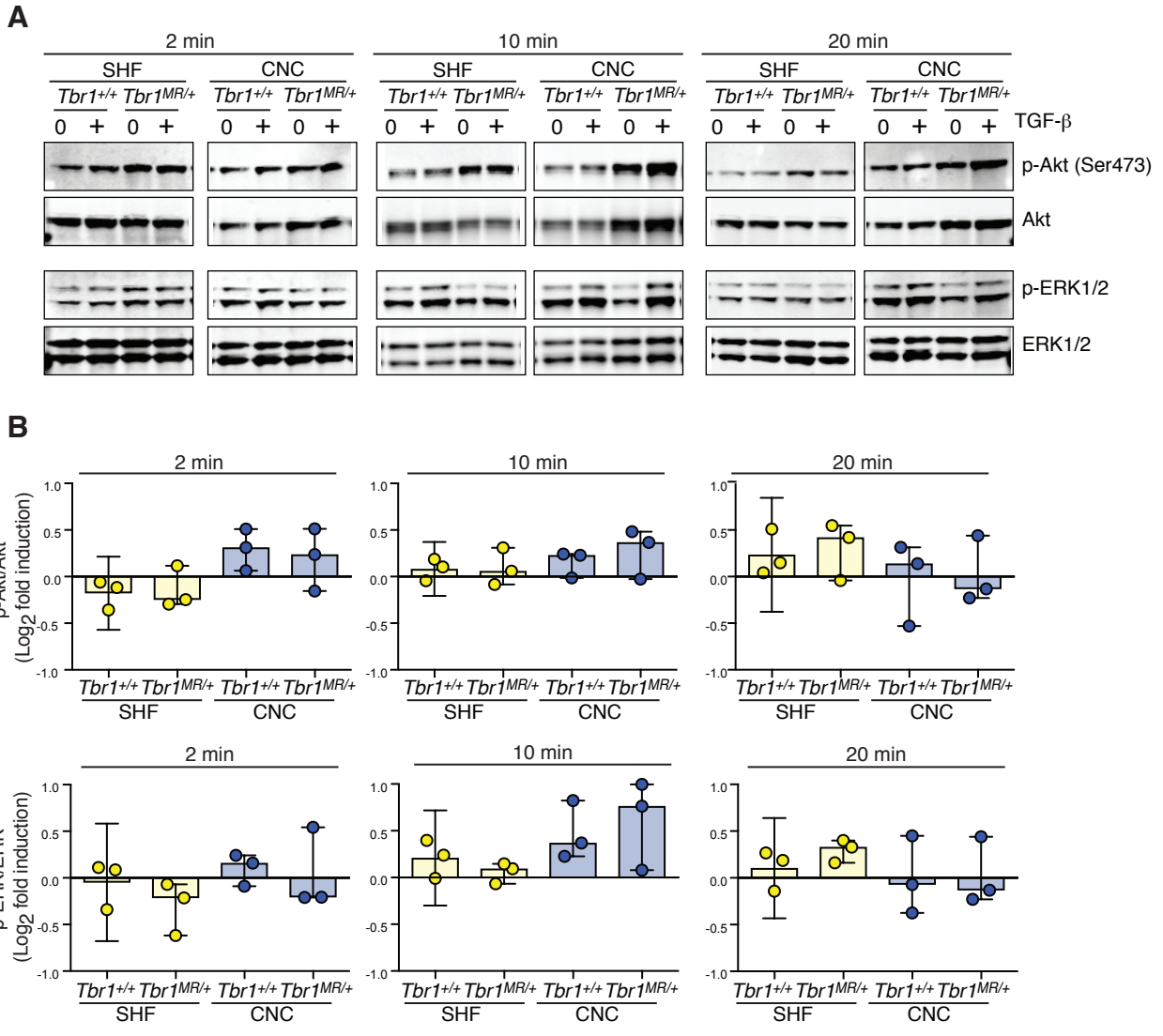

Supplementary Figure 2. Similar induction of non-Smad pathways in control and mutant SHF- and CNC-derived VSMCs.

(**A**) Representative immunoblot of protein lysates from serum-starved SHF- and CNC-derived VSMCs from mice of the indicated genotypes in the absence or presence of TGF-β1 (10 ng/ml) for the indicated duration. Levels of p-ERK (Thr202/Tyr204) and p-Akt (Ser473) were assessed and quantified (**B**) using antibodies specific for the respective phosphorylated form and normalized to total protein (n=3 for each condition). No significant differences were found. Numerical data are presented as scatter dot-plots with boxes, with the box denoting the mean; error bars identify the 95% confidence interval.

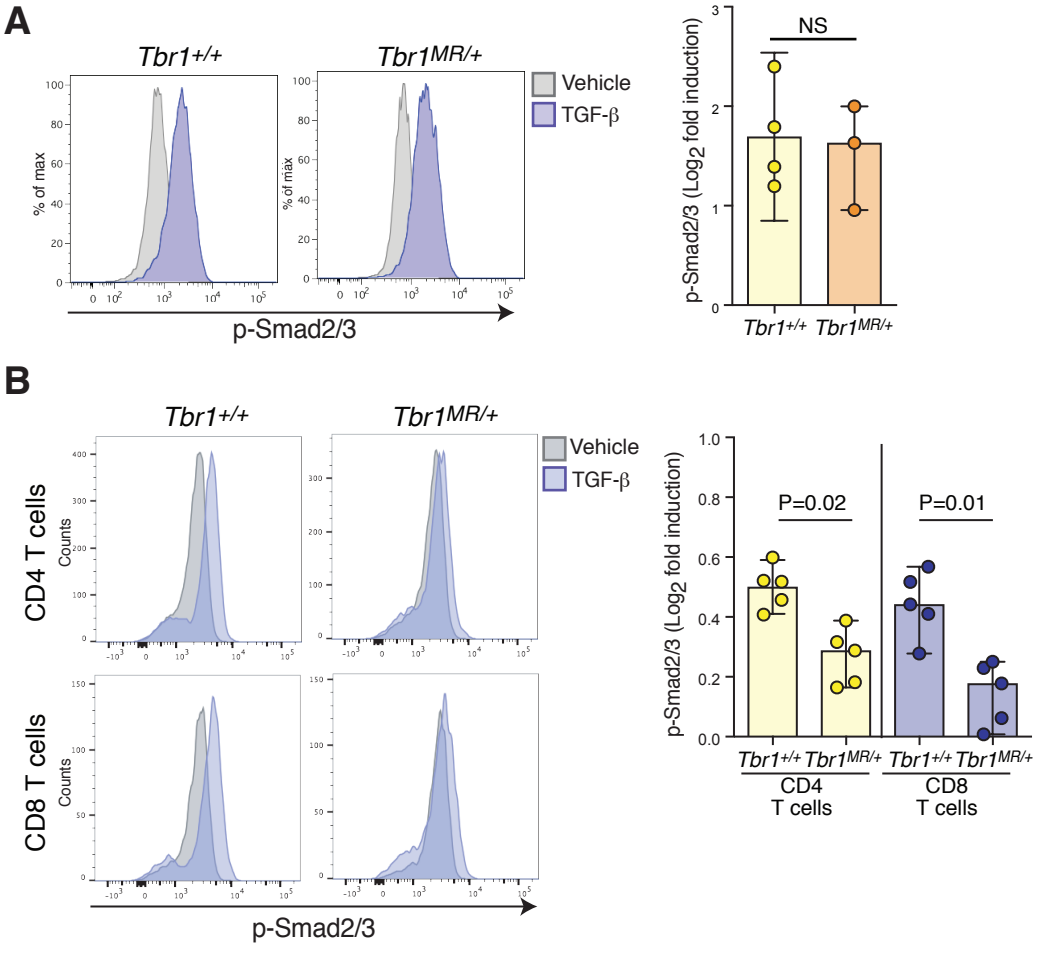

Supplementary Figure 3. TGF-β-dependent induction of Smad2/3 phosphorylation in adventitial fibroblasts and T lymphocytes from control and *Tbr1*$^{MR/+}$ LDS mice.
(**A**) Flow cytometry histogram plots and quantification of p-Smad2/3 induction over baseline in serum-starved adventitial fibroblasts from mice of the indicated genotypes after exposure to 1 ng/ml of TGF-β1 for 1 hour. Levels of p-Smad2/3 were assessed by phospho-flow cytometry using an antibody specific for p-Smad2/3 (control n=4, mutant n=3); no significant differences were found. (**B**) Flow cytometry histogram plots and quantification of p-Smad2/3 induction over baseline in CD4^{+} and CD8^{+} T cells isolated from the spleen of mice of the indicated genotypes and stimulated with 0.5 ng/ml of TGF-β1 for 30 minutes. Levels of p-Smad2/3 were assessed by phospho-flow cytometry using an antibody specific for p-Smad2/3 (control n=5, mutant n=5). All *P* values refer to Kruskal-Wallis test with FDR-based multiple comparison correction. Numerical data are presented as scatter dot-plots with boxes, with the box denoting the mean; error bars identify the 95% confidence interval. NS, not significant.

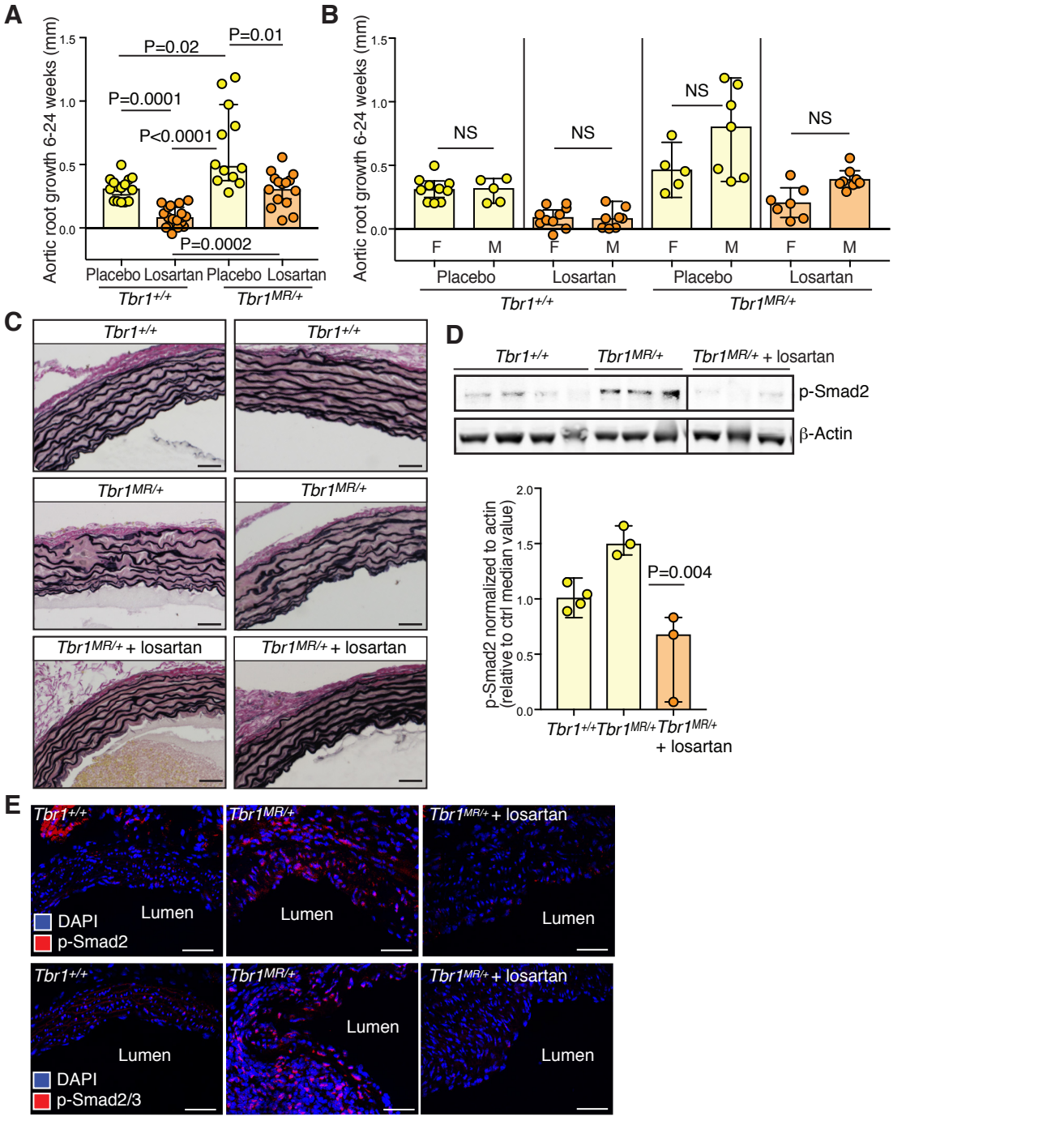

Supplementary Figure 4. Treatement with losartan associates with reduced aortic root growth and p-Smad2/3 levels in the aortic root of *Tbr1*$^{MR/+}$ mice. (**A**) Aortic root growth rate in control (*Tbr1*$^{+/+}$) and mutant (*Tbr1*$^{MR/+}$) mice treated with placebo or losartan (100 mg/kg/day) from 6 to 24 weeks of age (control n=15, mutant n=12; losartan samples, control n=18, mutant n=15). *P* values refer to Kruskal-Wallis test with FDR-based multiple comparison correction. (**B**) No sex-specific differences ($P \leq 0.05$) were observed within any treatment group for data shown in panel A; F= females, M=males. (**C**) Representative Verhoeff-Van Gieson-stained sections from the aortic root of 24-week-old mice of the indicated treatment and genotype; scale bar is 40 µm. Experiment was performed at least 3 times. (**D**) Immunoblot of protein lysates from the aortic root of 24-week-old mice of the indicated treatment and genotype probed with antibodies that recognize p-Smad2 and β-actin; a black vertical line separates lanes that were run on the same gel but were noncontiguous. Diagram shows levels of p-Smad2 after normalization to β-actin; *P* values refer to 1-way ANOVA followed by Holm-Sidak's multiple comparisons test. (**E**) Representative IF images of the aortic root of 24-week-old control and mutant mice stained with an antibody that recognizes p-Smad2 or with an unrelated antibody that recognizes p-Smad2/3; scale bar is 50 µm. Experiment was performed at least 3 times. Image enhancement for visual display was applied uniformly to all panels. Numerical data are presented as scatter dot-plots with boxes, with the box denoting the mean; error bars identify the 95% confidence interval. NS, not significant.

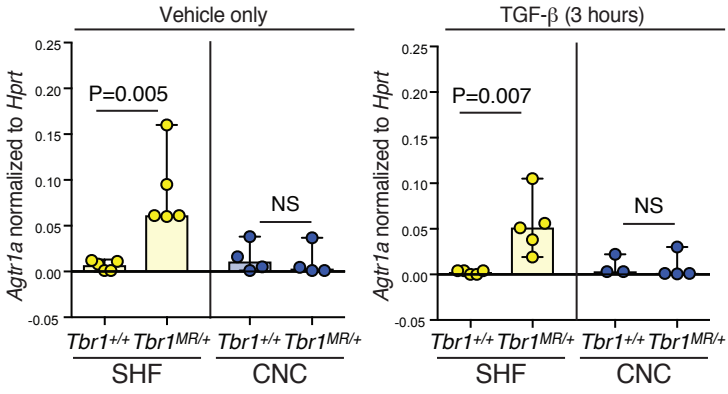

Supplementary Figure 5. Upregulation of *Agtr1a* in SHF-, but not CNC-derived primary VSMCs from *Tbr1*$^{MR/+}$ mice. Normalized *Agtr1a* mRNA expression in serum-starved SHF- and CNC-derived VSMCs from control (*Tbr1*$^{+/+}$) and mutant (*Tbr1*$^{MR/+}$) mice cultured in the presence or absence of TGF-β1 (10 ng/ml) for 3 hours; SHF samples: control n=5, mutant n=5; CNC samples, control n=4 (one not detectable after 3 hours of TGF-β treatment), mutant n=4; *P* values refer to Kruskal-Wallis test with FDR-based multiple comparison correction. Numerical data are presented as scatter dot-plots with boxes, with the box denoting the mean; error bars identify the 95% confidence interval. NS, not significant.

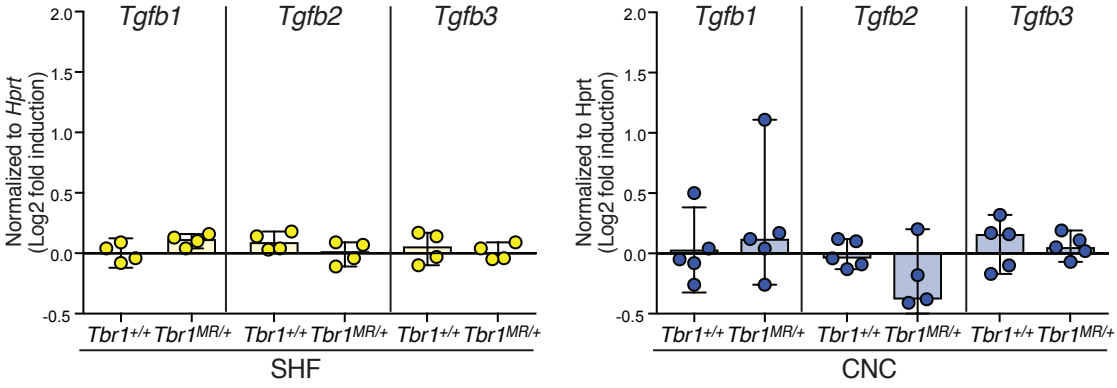

Supplementary Figure 6. Induction of *Tgfb* isoforms in SHF- and CNC-derived primary VSMCs after treatment with AngII for 3 hours. Induction of *Tgfb1*, *Tgfb2* and *Tgfb3* in serum-starved SHF- and CNC-derived VSMCs of the indicated genotype after exposure to AngII (10 μM) for 3 hours (SHF samples: control n=5, mutant n=4; CNC samples, control n=5, mutant n=5). No significant differences were found. Numerical data are presented as scatter dot-plots with boxes, with the box denoting the mean; error bars identify the 95% confidence interval.

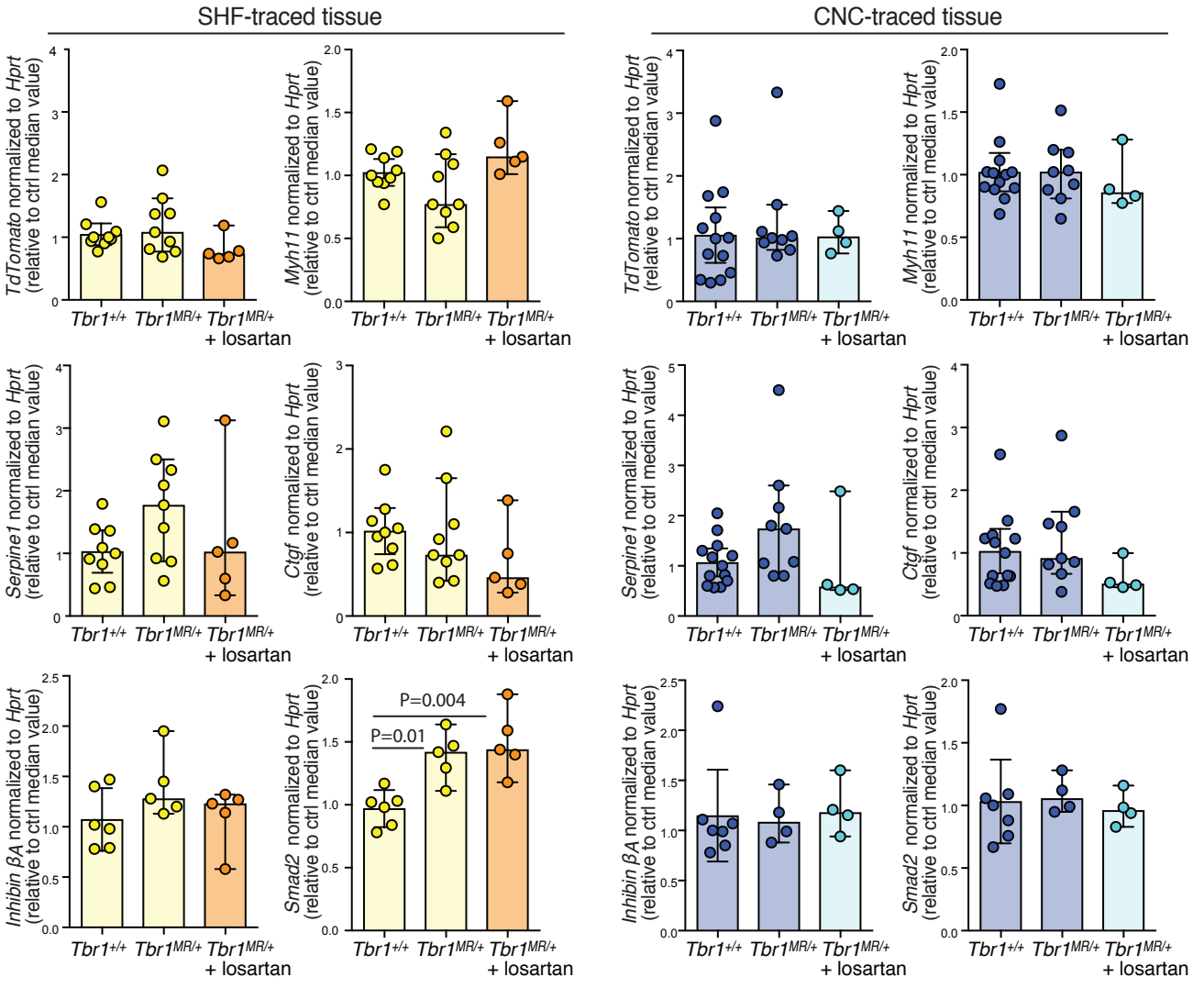

Supplementary Figure 7. Treatment with losartan does not result in downregulation of *Smad2* or *Inhibin βA* in either SHF- or CNC-derived aortic root tissue of *Tbr1*$^{MR/+}$ mice.
Expression of indicated transcripts in SHF- and CNC-derived aortic tissue obtained by laser-capture microdissection in 12-week-old lineage-traced mice of the indicated genotype and treatment (top two rows: SHF samples: control n=9, mutant n=9; losartan=5; CNC samples, control n=13, mutant n=9, losartan=4; bottom row: SHF samples: control n=6, mutant n=5; losartan=5; CNC samples, control n=7, mutant n=4, losartan=4). *P* values refer to Kruskal-Wallis test with FDR-based multiple comparison correction. Numerical data are presented as scatter dot-plots with boxes, with the box denoting the mean; error bars identify the 95% confidence interval.

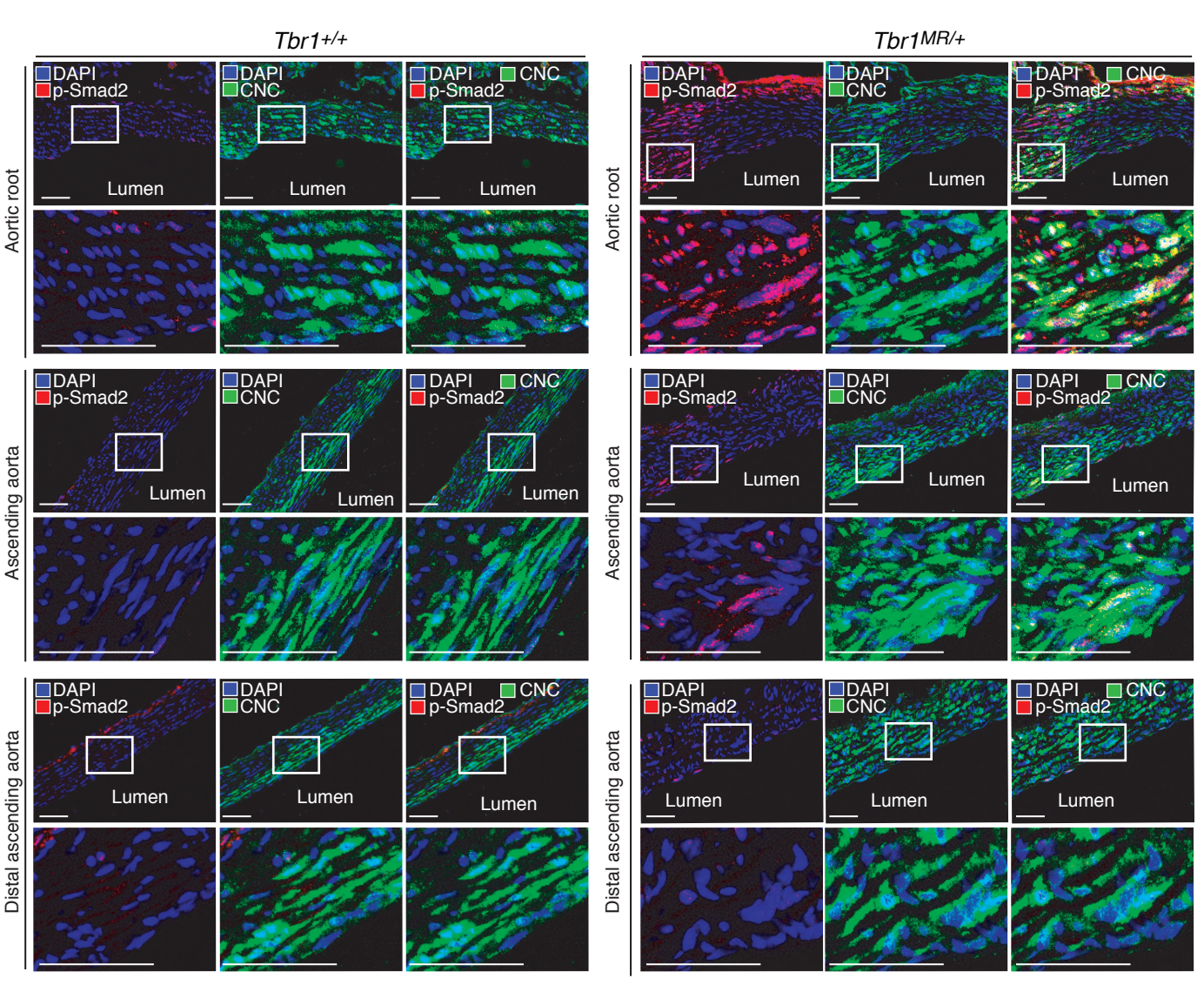

Supplementary Figure 8. Smad2 phosphorylation is enriched in CNC-derived tissue in the aortic root media but not in the distal ascending aorta of *Tbr1*$^{MR/+}$ mice.
Representative IF images showing staining for p-Smad2 in the aortic root and ascending aorta of 12-week-old control (*Tbr1*$^{+/+}$) and mutant (*Tbr1*$^{MR/+}$) mice in which CNC-derived tissue is marked by expression of YFP; insets mark areas shown at higher magnification below each panel; scale bar is 50 μm. Image enhancement for visual display was applied uniformly to all panels. Experiment was conducted at least 3 times.

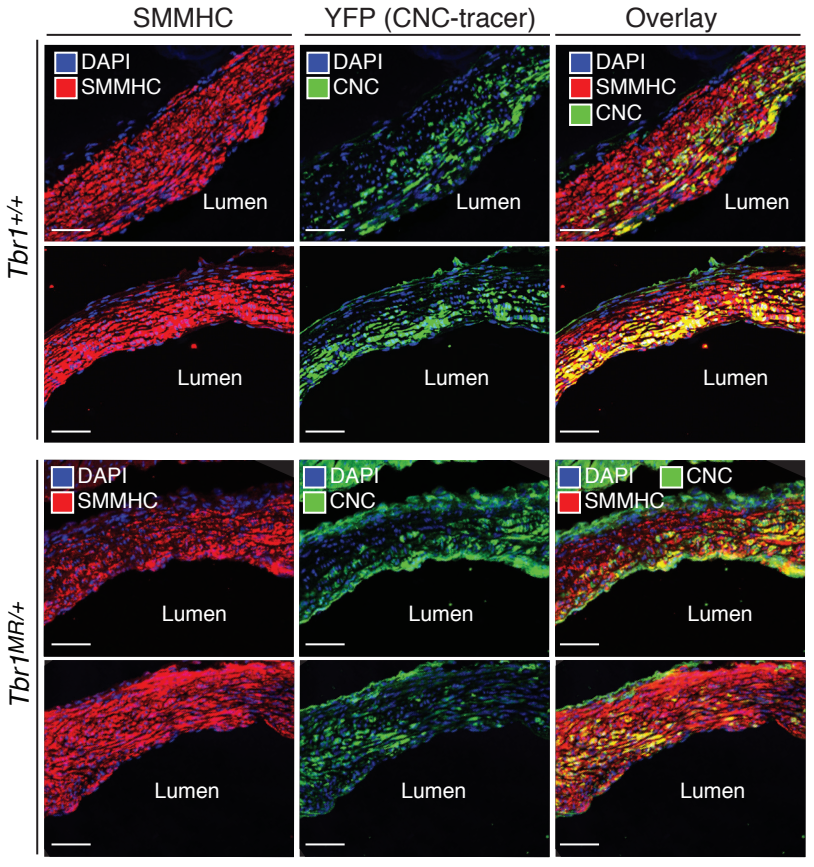

Supplementary Figure 9. Overlap between CNC-derived and smooth muscle myosin heavy chain (SMMHC)-positive cells in the aortic root media of control and *Tbr1*$^{MR/+}$ mice.
Representative IF images showing staining for the smooth muscle cell marker SMMHC in the aortic root of 12 week-old control (*Tbr1*$^{+/+}$) and mutant (*Tbr1*$^{MR/+}$) mice in which CNC-derived tissue is marked by expression of YFP; scale bar is 50 μm. Image enhancement for visual display was applied uniformly to all panels. Experiment was conducted at least 3 times.

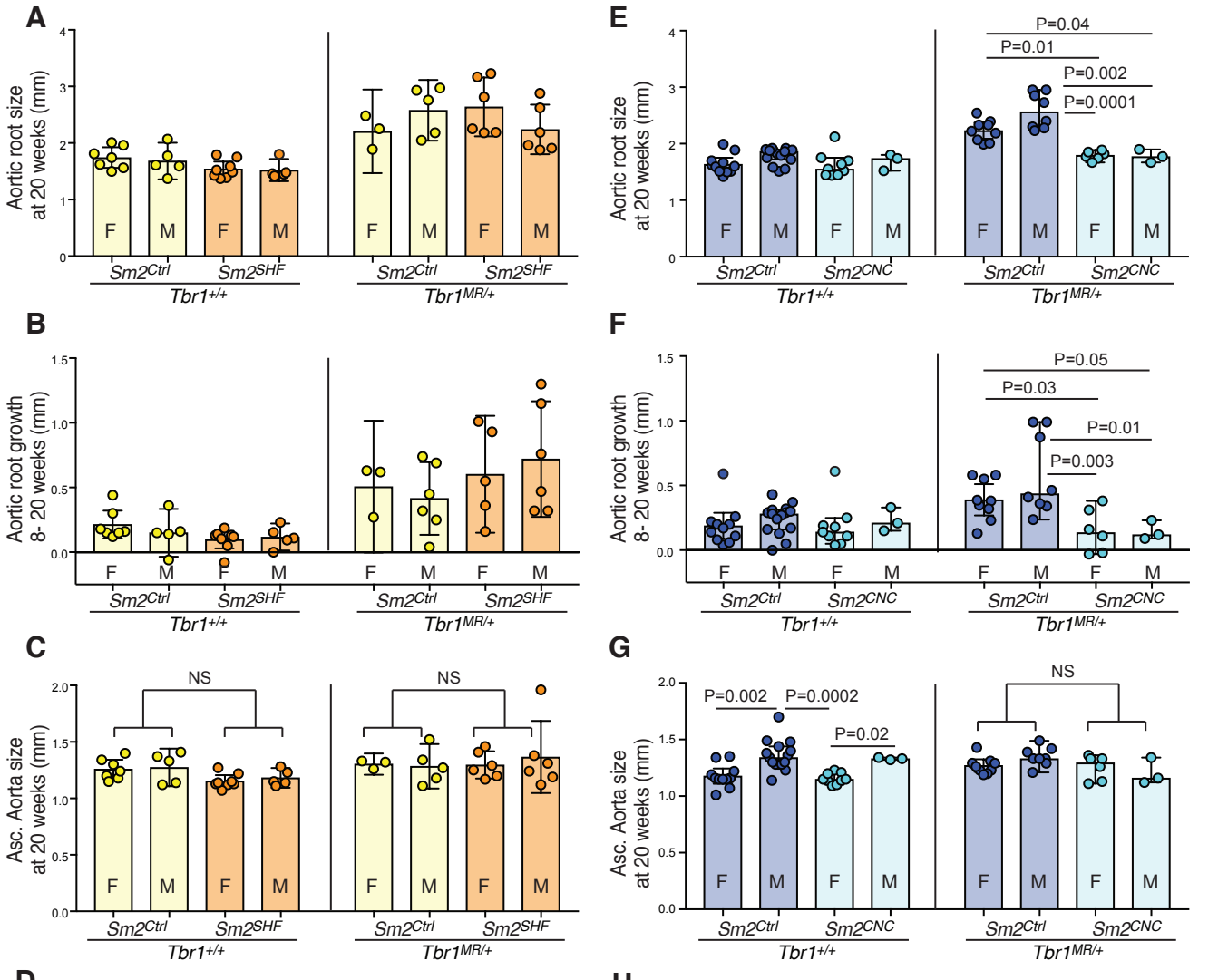

D

Genotype	*Tbr1*$^{+/+}$	*Tbr1*$^{+/+}$*; Sm2*^{SHF}	*Tbr1*$^{MR/+}$	*Tbr1*$^{MR/+}$*; Sm2*^{SHF}
dead/total	0/12	0/13	2/10	1/13
% survival	100%	100%	80%	92%

H

Genotype	*Tbr1*$^{+/+}$	*Tbr1*$^{+/+}$*; Sm2*^{CNC}	*Tbr1*$^{MR/+}$	*Tbr1*$^{MR/+}$*; Sm2*^{CNC}
dead/total	0/26	1/13	1/18	1/10
% survival	100%	92%	94%	90%

Supplementary Figure 10. Deletion of *Smad2* in SHF- or CNC-derived cells does not result in sex-specific aortic root effects, nor aneurysm of the ascending aorta.
Aortic root size (**A**) and growth rate (**B**) in 20 week-old female (F) and male (M) control (*Tbr1*$^{+/+}$) and mutant (*Tbr1*$^{MR/+}$) mice in which *Smad2* (*Sm2*) is not deleted (*Sm2*^{Ctrl}) or deleted in SHF-derived cells (*Sm2*^{SHF}). (**C**) Diameter of the proximal ascending aorta of 20 week-old mice of the indicated genotype. (**D**) Survival for mice of the indicated genotypes during the observational period (from 8 to 20 weeks of age); no significant differences were found by exact contingency test. Aortic root size (**E**) and growth rate (**F**) in 20 week-old mice of the indicated genotype in which *Smad2* (*Sm2*) is not deleted (*Sm2*^{Ctrl}), or deleted in CNC-derived cells (*Sm2*^{CNC}). (**G**) Diameter of the proximal ascending aorta in 20 week-old female and male mice of the indicated genotypes. This was the only cohort where sex-specific differences were found. (**H**) Survival for mice of the indicated genotypes during the observational period (from 8 to 20 weeks of age); no significant differences were found by exact contingency test. For all groups n ≥3; *P* values refer to Kruskal-Wallis test with FDR-based multiple comparison correction. Numerical data are presented as scatter dot-plots with boxes, with the box denoting the mean; error bars identify the 95% confidence interval. NS, not significant.

Supplementary Table 1.
This table lists the sex of all samples shown in figures and supplementary figures; M=male and F= female.

Figure 1	**Control *Tbr1*$^{+/+}$**	**Mutant *Tbr1*$^{MR/+}$**
A	F=1; M=0	F=0; M=1
B	F=13; M=12	F=10; M=6
C	F=1, M=0	F=0, M=1
D	F=0; M=1	F=0; M=1
E	F=0; M=1	F=1; M=0
F	F=0; M=3	F=0; M=3

Figure 2	**Control *Tbr1*$^{+/+}$**	**Mutant *Tbr1*$^{MR/+}$**
A	F=0; M=3	F=0; M=3
B	F=1; M=0	F=0; M=1

Figure 3	**Control *Tbr1*$^{+/+}$**		**Mutant *Tbr1*$^{MR/+}$**	
	SHF-derived	**CNC-derived**	**SHF-derived**	**CNC-derived**
C	F=0; M=1	F=1 M=0	F=0; M=1	F=1 M=0

Figure 4	**Control *Tbr1*$^{+/+}$**		**Mutant *Tbr1*$^{MR/+}$**	
	SHF-derived	**CNC-derived**	**SHF-derived**	**CNC-derived**
A	F=3; M=2	F=2; M=3	F=2; M=2	F=2; M=3
B	F=2; M=1	F=2; M=1	F=1; M=2	F=2; M=1
C	F=2; M=2	F=2; M=2	F=1; M=3	F=2; M=2

Figure 5	**Control *Tbr1*$^{+/+}$**		**Mutant *Tbr1*$^{MR/+}$**	
	SHF-derived	**CNC-derived**	**SHF-derived**	**CNC-derived**
A	F=3; M=2	F=2; M=2	F=2; M=3	F=2; M=2
B	F=2; M=3	F=2; M=2	F=1; M=3	F=2; M=2
C	F=1; M=0	F=0; M=1	F=0; M=1	F=0; M=1
D	F=2; M=3	F=2; M=3	F=1; M=3	F=1; M=4

Figure 6	**Control *Tbr1*$^{+/+}$**	**Mutant *Tbr1*$^{MR/+}$**	
B-SHF	F=5; M=4	F=3; M=6	LOS F=3; M=2
B-CNC	F=3; M=10	F=5; M=4	LOS F=3; M=1

Figure 7	**Control *Tbr1*$^{+/+}$**	**Mutant *Tbr1*$^{MR/+}$**
A	F=0 M=1	F=1, M=0
B	F=0 M=1	F=1, M=0

Figure 8	**Control *Tbr1*$^{+/+}$**			**Mutant *Tbr1*$^{MR/+}$**		
	Control	**Smad2^{SHFcKO}**	**Smad2^{CNC}**	**Control**	**Smad2^{SHFcKO}**	**Smad2^{CNCcKO}**
A	F=7, M=5	F=8, M=5		F=3, M=5	F=6, M=6	
B	F=11, M=15		F=9, M=3	F=9, M=8		F=6, M=3
C	F=1, M=2	F=2, M=1	F=1, M=2	F=1, M=2	F=1, M=2	F=0, M=3
D	F=0, M=3	F=1, M=2	F=1, M=2	F=0, M=3	F=0, M=3	F=1, M=2

Figure 9	**Control *Tbr1*$^{+/+}$**	**Mutant *Tbr1*$^{MR/+}$**		
	Control	**Control**	**Smad2^{SHFcKO}**	**Smad2^{CNCcKO}**
A	F=2; M=0	F=2; M=0	F=1; M=1	
B	F=0; M=2	F=0; M=2		F=0; M=2

Sup. Fig. 1	Control *Tbr1*$^{+/+}$		Mutant *Tbr1*$^{MR/+}$	
	SHF-derived	**CNC-derived**	**SHF-derived**	**CNC-derived**
A	F=2; M=3	F=2 M=2	F=2; M=3	F=2 M=3
B	F=1; M=3	F=2 M=3	F=2; M=3	F=2 M=3
C	F=2; M=2	F=2 M=2	F=2; M=3	F=2 M=3

Sup. Fig. 2	Control *Tbr1*$^{+/+}$	Mutant *Tbr1*$^{MR/+}$		
	SHF-derived	**CNC-derived**	**SHF-derived**	**CNC-derived**
	F=1; M=2	F=1 M=2	F=2; M=1	F=2 M=1

Sup. Fig. 3	Control *Tbr1*$^{+/+}$	Mutant *Tbr1*$^{MR/+}$
A	F=3; M=1	F=1; M=2
B	F=0; M=5	F=0; M=5

Sup. Fig. 4	Control *Tbr1*$^{+/+}$		Mutant *Tbr1*$^{MR/+}$	
A	F=10; M=5	LOS: F=10; M=8	F=5; M=7	LOS: F=7; M=8
B	F=10; M=5	LOS: F=10; M=8	F=5; M=7	LOS: F=7; M=8
C	F=1; M=1		F=1; M=1	LOS=1; M=1
D	F=3; M=1		F=3; M=0	LOS: F=1; M=2
E	F=1; M=0		F=1; M=0	LOS F=0; M=1

Sup. Fig. 5	Control *Tbr1*$^{+/+}$		Mutant *Tbr1*$^{MR/+}$	
	SHF-derived	**CNC-derived**	**SHF-derived**	**CNC-derived**
	F=3; M=2	F=2; M=2	F=2; M=3	F=2; M=2

Sup. Fig. 6	Control *Tbr1*$^{+/+}$		Mutant *Tbr1*$^{MR/+}$	
	SHF-derived	**CNC-derived**	**SHF-derived**	**CNC-derived**
	F=2; M=3	F=2; M=3	F=1; M=3	F=1; M=4

Sup. Fig. 7	Control *Tbr1*$^{+/+}$	Mutant *Tbr1*$^{MR/+}$	
SHF	F=5; M=4 (last row F=3; M=3)	F=3; M=6 (last row F=2; M=3)	LOS F=3; M=2
CNC	F=3; M=10	F=5; M=4	LOS F=3; M=1

Sup. Fig. 8	Control *Tbr1*$^{+/+}$	Mutant *Tbr1*$^{MR/+}$
	F=1 M=0	F=1, M=0

Sup. Fig. 9	Control *Tbr1*$^{+/+}$	Mutant *Tbr1*$^{MR/+}$
	F=1 M=1	F=2, M=0